Available online at www.sciencedirect.com
SCIENCE DIRECT®
International Journal of Thermal Sciences 42 (2003) 591–604
International Journal of Thermal Sciences
www.elsevier.com/locate/ijts

Numerical study of a piston-driven laminar flow and heat transfer in a pipe with a sudden expansion

Ayda Boughamoura [a], Hafedh Belmabrouk [b], Sassi Ben Nasrallah [a,*]

[a] *École nationale d'ingénieurs de Monastir, laboratoire d'études des systèmes thermiques et énergétiques, avenue Ibn Eljazar, 5019 Monastir, Tunisia*
[b] *Faculté des sciences de Monastir, département de physique, 5000 Monastir, Tunisia*

Received 3 December 2001; accepted 31 August 2002

Abstract

The present paper deals with the numerical investigation of piston-driven heat transfer and fluid flow in a cylinder containing a sudden expansion. The calculation procedure employed is based on a control-volume-based finite element method for incompressible flow with a staggered and moving grid and SIMPLER algorithm for pressure-velocity coupling. The numerical results show a good agreement with the experimental data reported in the literature. Results concerning time and space evolution of the thermal and flow fields downstream and upstream of the sudden expansion are presented for different values of the expansion ratio, the initial clearance volume, and the piston velocity. The effects of these parameters on the instantaneous convective heat flux and on the total convected heat are also evaluated at the sudden expansion section.

Keywords: Numerical simulation; Heat transfer; Piston-driven unsteady laminar flow

1. Introduction

Because of its importance in reciprocating machines (Stirling engines, reciprocating compressors, internal combustion engines, and hydraulic pumps ...), piston-driven flow within a cylinder has received increasing attention.

Among the published works dealing with this flow type we cite those of Heywood [1], Ahmadi-Befrui et al. [2], Farhanieh et al. [3], and Mao et al. [4] concerning turbulent flow in geometries close to those of internal combustion engines and those of Durst et al. [5] and Ströll et al. [6,7] concerning piston-driven laminar flow in a pipe-assembly with a sudden expansion.

The work of Durst et al. [5] deals with an experimental study of the flow field generated by the piston movement during the intake stroke in a pipe-assembly with sudden expansion. In the experiments the piston, which closes the larger pipe, is put abruptly in movement from rest to a constant velocity. Flow visualization and LDA measurements are the techniques used in the investigation. The presented results, obtained by the flow visualization and LDA measurement techniques, concern the effects of the piston velocity and the initial clearance volume. These results show that under some conditions, secondary vortices can occur downstream the sudden expansion.

The work of Ströll et al. [6] is a numerical investigation based on a finite volume method. All results are obtained with a constant piston velocity $U_p = 11.9$ mm·s^{-1} corresponding to a Reynolds number of 98, an initial clearance $L_0 = 40$ mm, an expansion ratio between the inlet pipe and the cylinder radiuses $\alpha = 0.5$ and a total piston stroke $C = 24.3$ mm. With these conditions, secondary vortices cannot emerge and only the primary vortex is generated.

Although, many reciprocating engines encountered in practice involve a change in temperature, only an isothermal flow was considered by Durst et al. [5] and by Ströll et al. [6, 7]. These investigations were restricted to isothermal flows and focused on the flow field without considering the heat transfer. So, the aim of the present paper is to complements the works of Durst et al. [5] and Ströll et al. [6,7] using numerical predictions by considering a nonisothermal flow during the intake stroke and by determining the expansion ratio and the piston velocity effects on the flow and thermal fields.

* Corresponding author.
E-mail address: ayda.boughamoura@issatso.rnu.tn (A. Boughamoura).

1290-0729/03/$ – see front matter
doi:10.1016/S1290-0729(03)00025-5

Nomenclature

C	total piston stroke	m
$\%C$	relative piston stroke, $= 100\frac{L_2-L_0}{C}$	
C_p	specific heat at constant pressure	$J{\cdot}kg^{-1}{\cdot}K^{-1}$
C_v	specific heat at constant volume	$J{\cdot}kg^{-1}{\cdot}K^{-1}$
Fc	instantaneous convective heat flux	W
Fct	total convected heat	J
$\boldsymbol{J}$	combined convection–diffusion flux	J
$\boldsymbol{J}_c$	convection flux	J
$\boldsymbol{J}_d$	diffusion flux	J
L_0	initial clearance	m
L_1	inlet tube length	m
L_2	larger pipe instantaneous length	m
p	local pressure	Pa
Pr	Prandtl number	
$\Re$	gas constant of air (perfect gas)	$J{\cdot}kg^{-1}{\cdot}K^{-1}$
R_1	inlet-pipe radius	m
R_2	larger pipe radius	m
Re	Reynolds number	
S_Φ	volumetric source term	
t	time	s
T	dimensionless temperature	
tc	compression ratio, $= (L_0 + C)/L_0$	
T_{moy}	instantaneous mean temperature into the larger pipe	K
$\boldsymbol{U}$	fluid velocity vector	$m{\cdot}s^{-1}$
U	velocity component on z direction	$m{\cdot}s^{-1}$
$\boldsymbol{U}_g$	instantaneous grid velocity	$m{\cdot}s^{-1}$
$\boldsymbol{U}_r$	relative velocity or fluid velocity on the moving coordinate system, $= U - U_g$	$m{\cdot}s^{-1}$
V	velocity component on r direction	$m{\cdot}s^{-1}$
U_p	piston velocity	$m{\cdot}s^{-1}$
z, r	cylinder coordinates	m

Greek letters

α	expansion ratio, $= R_1/R_2$	
δV	control volume	m^3
δt	time step	s
γ	ratio between C_p and C_v	
Φ	general physical variable	
Γ_Φ	diffusion coefficient	
λ	thermal conductivity	$W{\cdot}m^{-1}{\cdot}K^{-1}$
μ	dynamic viscosity	$kg{\cdot}m^{-1}{\cdot}s^{-1}$
ρ	density	$kg{\cdot}m^{-3}$
$\boldsymbol{\nabla}$	nabla operator	

Subscripts

i	value of the physical variable in the node i
0	initial value of the physical variable (at $t = 0$)

Superscripts

n	new time level (instant $t + \delta t$)
o	old time level (instant t)

The numerical method is of control-volume-based finite element type using a staggered and moving grid. The computed velocity profiles show a good agreement with the measurements of Ströll et al. [6]. The time and space evolutions of the thermal and flow fields are presented for different values of the expansion ratio, the clearance volume, and the piston velocity. The effects of these parameters on the instantaneous convective heat flux and on the total convected heat are also evaluated at the sudden expansion section.

2. Problem formulation

The problem geometry and the coordinate system are depicted in Fig. 1. The calculation domain consists of an inlet-pipe, a larger pipe and a moving piston. The inlet-pipe has a radius R_1 and length L_1, and the larger pipe has a radius R_2 ($R_2 > R_1$) and length $L_2(t)$ depending on time. The piston closes the larger pipe and its position varied between initial clearance L_0 and maximum clearance $(L_0 + C)$ as a function of time, where C is the total piston stroke. In the present study, only linear variation (constant piston velocity) [6] was considered.

An abruptly accelerated piston movement induces the flow. When the piston moves the fluid is sucked through the inlet-pipe into the larger pipe until the piston reaches the maximum clearance.

All numerical results were obtained for a constant piston velocity. The piston was impulsively started at $t = 0$, i.e., within the first time step it was accelerated from rest to the velocity $U_p = U_0$.

2.1. Governing equations

With reference to Newtonian incompressible fluid of constant physical properties and the cylindrical coordinates, the dimensionless form of continuity, momentum and energy equation are expressed into a common form:

$$\frac{\partial(\rho\Phi)}{\partial t} + \frac{\partial(\rho U\Phi)}{\partial z} + \frac{1}{r}\frac{\partial(r\rho V\Phi)}{\partial r} = \Gamma_\Phi\left[\frac{\partial^2\Phi}{\partial z^2} + \frac{1}{r}\frac{\partial}{\partial r}\left(r\frac{\partial\Phi}{\partial r}\right)\right] + S_\Phi \quad (1)$$

Where Φ represents the general dependent variable, z and r are the axial and the radial coordinates, respectively, with corresponding velocity components U and V, Γ_Φ is a diffusion coefficient, and S_Φ is the so-called source term.

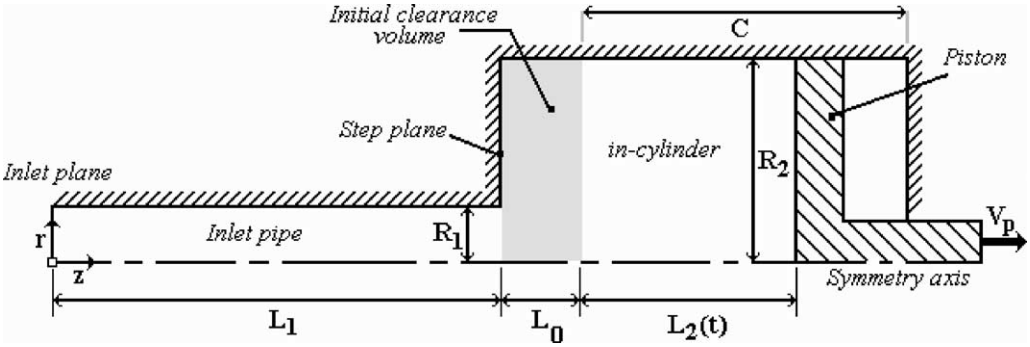

Fig. 1. Flow geometry with coordinate system and calculation domain.

For the Continuity equation:

$\Phi = 1, \quad \Gamma_\Phi = 0 \quad \text{and} \quad S_\Phi = 0$

For the z-momentum equation:

$\Phi = U, \quad \Gamma_\Phi = 1/Re \quad \text{and} \quad S_\Phi = -\partial p/\partial z$

For the r-momentum equation:

$\Phi = V, \quad \Gamma_\Phi = 1/Re \quad \text{and}$

$S_\Phi = -\partial p/\partial r - (2/Re)V/r^2$

For the energy equation:

$\Phi = T, \quad \Gamma_\Phi = 1/(RePr) \quad \text{and} \quad S_\Phi = 0$

This equation can be written also in vector form:

$$\frac{\partial(\rho\Phi)}{\partial t} + \operatorname{div}(\boldsymbol{J}) = S_\Phi \tag{2}$$

where $\boldsymbol{J}$ is the combined convection-diffusion flux:

$\boldsymbol{J} = \boldsymbol{J}_c + \boldsymbol{J}_d, \qquad \boldsymbol{J}_c = \rho U \Phi, \qquad \boldsymbol{J}_d = -\Gamma_\Phi \nabla \Phi$

where $\boldsymbol{U}$ is the fluid velocity vector.

In the above equations the space coordinate, the velocity, the time and the local pressure are respectively normalized with the larger pipe diameter ($2R_2$), the piston velocity ($U_p = U_0$), the characteristic time ($t_0 = 2R_2/U_0$) and the characteristic pressure (ρU_0^2). The expression of the dimensionless temperature is: $T = (T^* - T_0^*)/(T_e^* - T_0^*)$, where T_0^* is the initial temperature ($t = 0$) and T_e^* denotes the temperature at the inlet plane ($z = 0$).

The dimensionless numbers rising here are:

Reynolds number:

$$Re = \frac{\rho 2 R_2 U_0}{\mu}$$

Prandtl number:

$$Pr = \frac{\mu C_p}{\lambda}$$

2.2. Boundary and initial conditions

The air in the calculation domain is initially at rest and at a constant temperature T_0^*. In dimensionless term we have in all the calculation domain: $T = 0$ and $U = V = 0$ at $t = 0$.

For all wall boundaries, the no-slip condition was applied:

$U = U_p(t) \quad \text{and} \quad V = 0 \quad \text{at } z(t) = L_1 + L_2(t)$
$U = V = 0 \quad \text{at } r = R_1 \text{ and } 0 \leqslant z \leqslant L_1$
$U = V = 0 \quad \text{at } R_1 \leqslant r \leqslant R_2 \text{ and } z = L_1$
$U = V = 0 \quad \text{at } r = R_2 \text{ and } L_1 \leqslant z \leqslant L_1 + L_2(t)$

Along the centerline ($r = 0$), the normal gradient of the axial velocity and the radial velocity were set to zero: $\frac{\partial U}{\partial r} = 0$, $V = 0$.

At the inlet plane ($z = 0$), the radial velocity component is set to zero and the axial velocity is taken uniform, satisfying the global continuity requirement as determined by the piston velocity $U_p(t)$:

$$U(z = 0, t) = \left(\frac{R_2}{R_1}\right)^2 U_p(t) \tag{3}$$

For the temperature, the entering fluid (at the inlet plane) is set at a higher temperature $T_e^* = 333$ K than the air initially in the calculation domain $T_0^* = 303$ K. In dimensionless form we have: $T_e = T(z = 0) = 1$. All the wall boundaries are taken as adiabatic and along the centerline the normal gradient of the temperature is set to zero.

2.3. Numerical method and solution procedure

The governing equations are discretised with a control-volume-based finite element method (CVFEM) by adapting and extending ideas from CVFEMs proposed by Baliga and Patankar [8,9], Schneider and Raw [10], Masson et al. [11] and Omri and Ben Nasrallah [12].

The longitudinal cross-section plane is first divided into three-node triangular elements. Then the centroids of the elements are joined to the midpoints of the corresponding sides. This creates polygonal control volumes or cells around each node in the finite element grid (Figs. 2 and 3). The discretization of the longitudinal cross-section is rotated through 2π radians about the axis of symmetry. The result is a discretization of the axisymmetric calculation domain into torus elements of triangular cross-section and torus control volumes of polygonal cross-section.

In the present study, the calculation domain can be divided into two parts: the inlet-pipe and the larger pipe. The

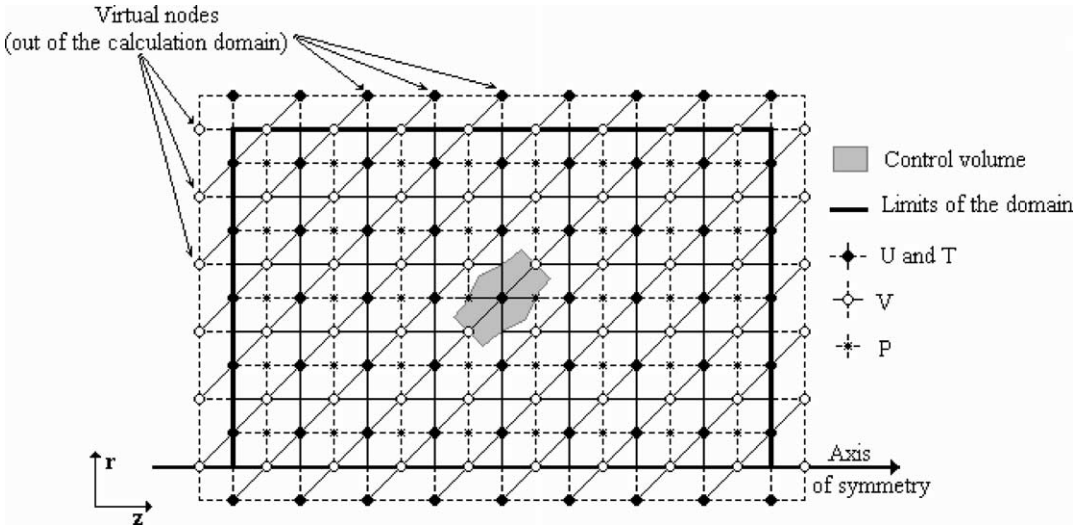

Fig. 2. Staggered numerical grid.

inlet-pipe has a constant volume and a fixed grid whereas the larger pipe deforms with the piston movement and has a volume depending on time and a moving grid. So the control volume in the larger pipe are changing with time. The grid velocity U_g giving a regular numerical grid at each instant is defined by:

$$U_g(z,t) = \begin{cases} 0 & \text{if } 0 \leqslant z \leqslant L_1 \\ \dfrac{z(t) - L_1}{L_2(t)} U_p(t) & \text{if } z \geqslant L_1 \end{cases} \tag{4}$$

To avoid oscillatory pressure and velocity fields, a staggered grid arrangement is employed [13], i.e., the axial velocity component and the temperature are stored at the same locations which are different from those of the radial velocity component and from those of the pressure (Fig. 2).

An integration of the conservation Eq. (2), when applied to the control volume (Fig. 3), leads to:

$$\int_t^{t+\delta t} \int_{iaob} \frac{\partial(\rho\Phi)}{\partial t} \,\mathrm{d}V\,\mathrm{d}t + \left[\int_t^{t+\delta t} \int_a^o J \cdot \boldsymbol{n} 2\pi r \,\mathrm{d}s\,\mathrm{d}t \int_t^{t+\delta t} \int_o^b J \cdot \boldsymbol{n} 2\pi r \,\mathrm{d}s\,\mathrm{d}t - \int_t^{t+\delta t} \int_{iaob} S_\Phi \,\mathrm{d}V\,\mathrm{d}t \right] + [\text{Similar contributions from other elements associated with node } i] = 0$$

Where $\boldsymbol{n}$ is a unit outward vector normal to the differential length element $\mathrm{d}s$.

In the derivation of algebraic approximations to surface integrals of convection and diffusion fluxes, the dependent variables U and V are interpolated linearly in each triangular element: $\Phi = Az + Br + C$. The constants A, B and C can

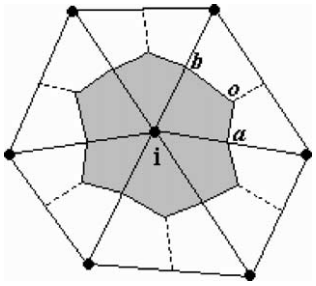

Fig. 3. Typical control volume associated to the node i.

be uniquely determined in terms of the (z, r) coordinates of the three nodes and the corresponding values of Φ. The temperature is interpolated linearly in diffusion terms and by a Flow-Oriented upwind scheme (FLO) [8,9] in convection terms; the interpolation function used in this scheme responds appropriately to an element-based Peclet number and to the direction of the element-average velocity vector.

The terms accounting explicitly for the grid movement are the temporal derivative. Integrating these terms yields:

$$\begin{aligned} &\int_t^{t+\delta t} \int_{iaob} \frac{\partial(\rho\Phi)}{\partial t} \,\mathrm{d}V\,\mathrm{d}t \\ &= \int_t^{t+\delta t} \frac{\partial}{\partial t} \left[\int_{iaob} (\rho\Phi) \,\mathrm{d}V \right] \mathrm{d}t - \int_t^{t+\delta t} \int_{iaob} \mathrm{div}(\rho\Phi \boldsymbol{U}_g) \,\mathrm{d}V\,\mathrm{d}t \\ &= \left[\rho^n \Phi_i^n \delta V^n - \rho^o \Phi_i^o \delta V^o \right] - \int_t^{t+\delta t} \int_{iaob} \mathrm{div}(\rho\Phi \boldsymbol{U}_g) \,\mathrm{d}V\,\mathrm{d}t \end{aligned} \tag{5}$$

where δV^0 and δV^n are the control volumes at old and new time levels respectively.

The convective fluxes are calculated with the relative velocity $\boldsymbol{U}_r = \boldsymbol{U} - \boldsymbol{U}_g$. The fixed grid region in the inlet-pipe can be considered as a special case, with zero grid velocity.

To link the pressure to the velocity field, the SIMPLER algorithm described by Patankar and Spalding [14] is employed. It makes use of a pressure correction equation derived from the continuity equation. An implicit scheme is used and at each time level the two momentum equations and the pressure correction equation were solved iteratively until convergent solutions were achieved. The iterations are terminated after overall accuracy has fallen below 0.1 percent. The scheme was then advanced in time.

A numerical grid of [121 × 51] uniformly distributed nodes was used for the entire calculation domain. The time increments chosen was $\Delta t = 0.001$ s, corresponding to a maximum piston displacement of 65 μm. This time interval was sufficiently small to obtain solutions not influenced by the time step.

3. Results and discussion

In order to validate the used control-volume-based finite element method (CVFEM), the numerical results are compared to the experimental results obtained by Ströll et al. [6] during the intake stroke with a constant piston-velocity and an isothermal fluid. Fig. 4, compares the predicted and the measured axial velocity profiles at the end of the intake stroke for successive z-locations inside the larger pipe. The agreement between the predicted and the measured profiles is very satisfactory. Hence, the present CVFEM based numerical code may be considered reliable.

In the next part, we present for the fixed geometric conditions ($R_2 = 22.5$ mm, $L_1 = 100$ mm and $C = 90$ mm) the numerical results of the fluid flow and the thermal field during the intake stroke. The effect of the expansion ratio (α), the clearance volume (L_0), and the piston velocity (Reynolds number) on the flow and thermal fields and on the instantaneous and the total convective heat fluxes is also carried out.

3.1. Flow field

Figs. 5, 6 and 7 present the predicted streamline patterns at different piston locations corresponding to 12.5%, 25%, 50% and 100% of the total piston stroke, and for different values of expansion ratio, clearance volume L_0 and Reynolds number respectively.

A series of streamline patterns for various piston displacements are shown in these figures. They provide an impression of the evolution of the flow structure during the intake stroke. As soon as the piston moves, the fluid is sucked through the inlet-pipe into the larger pipe. The induced inlet flow separates at the lip of the sudden expansion, forming a counter-clockwise rotating vortex. This vortex takes birth

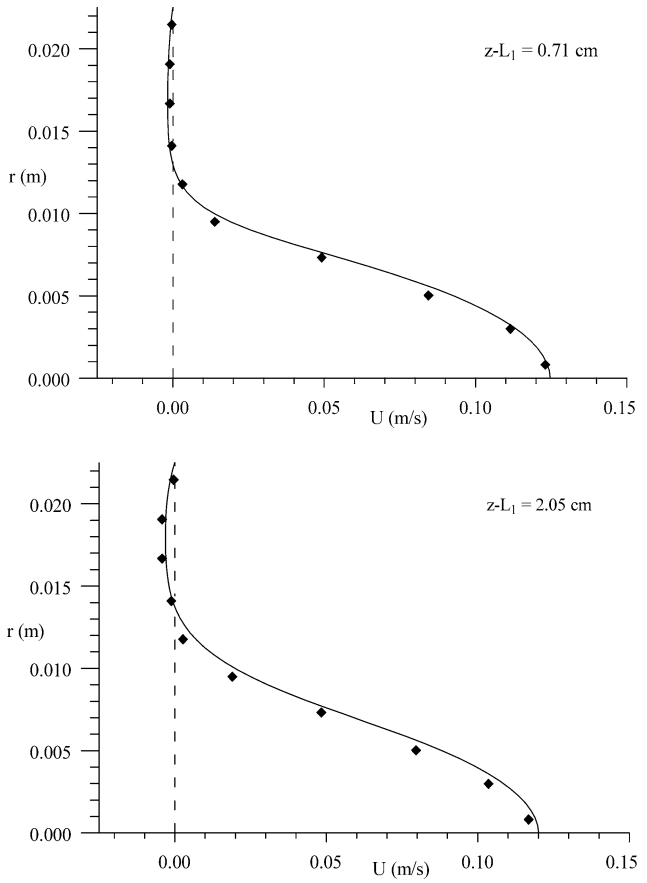

Fig. 4. Axial velocity profiles at the end of the intake stroke: —- predicted; ◆ measured [6].

by the generation of a positive vorticity by viscous separation [15–17]. Behind the separation bubbles, the streamlines of the inlet flow become strongly curved (Fig. 5(2(a))). This is due to a region of high pressure retarding the approaching flow and turning it in the r-direction. Indeed, due to their higher velocity, fluid elements moving along the centreline overcome the pressure gradient more easily than fluid element coming from the pipe wall region. Consequently, near the symmetry line the streamline patterns are almost parallel to the cylinder axis. Far from the centreline region, the fluid elements bear less kinetic energy and are more strongly retarded than the fluid elements near the symmetry axis. Consequently, the deflection in the r-direction becomes greater as the radius increases.

As can be seen from Figs. 5, 6 and 7, after forming close to the step plane the primary vortex is first elongated in the r-direction to reach the cylinder lateral wall. Then this vortex is convected towards the piston and becomes elongated axially in the z-direction as the piston moves along. As the piston approach its maximum location ($L_0 + C$), the primary vortex reaches the piston region and occupies the whole cylinder space.

Under some conditions a secondary vortex can appear, close the lateral wall, when the primary vortices reach the piston. The time of the appearance of these secondary vortices was function of the initial clearance volume (L_0),

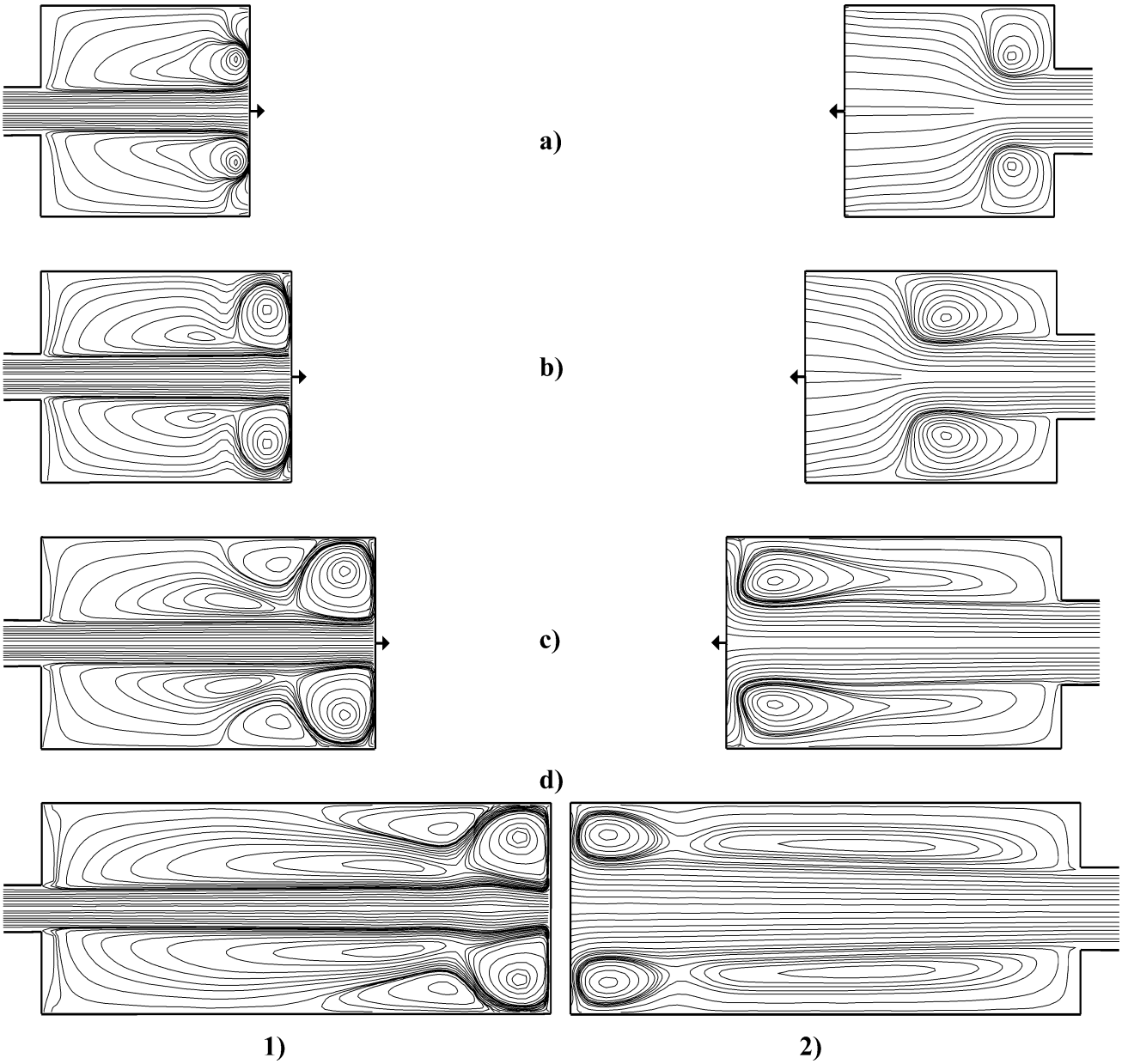

Fig. 5. Streamline patterns for different expansion ratios (α) during the intake stroke ($Re = 100$, $L_0 = 45$ mm): (1) $\alpha = 0.2$; (2) $\alpha = 0.4$: (a) 12.5%, (b) 25%, (c) 50%, (d) 100% of the piston stroke (C).

the expansion ratio (α) and the Reynolds number. The occurrence of multiple vortexes has been shown by Durst et al. [5] using the flow visualisation technique.

In this first part, we investigate the effect of the expansion ratio on the flow field by choosing two values of α: 0.2 and 0.4. By comparing the predicted streamline patterns at the beginning of the intake stroke for different values of $\alpha = R_1/R_2$ (Fig. 5(1(a)) and (2(a))), it appears that the size of the recirculating zone near the step plane decreases as the expansion ratio increases. According to Eq. (3), the inlet axial velocity is inversely proportional to the expansion ratio. Therefore, the weak kinetic energy of fluid elements when α is greater explains the great deflection of the main jet. When α is smaller, the fluid elements coming from the pipe wall region, which bear more kinetic energy, cover a greater distance before being carried into the recirculating region. In other words, as α decreases the vortex spreads in the r-direction towards the cylinder wall and axially towards the piston region more rapidly. According to Fig. 5, we can conclude that increasing the expansion ratio slows the flow field evolution.

For a small expansion ratio, the fluid elements coming from the intake pipe has a great velocity and so the forming primary vortex reaches rapidly the piston region. This vortex is forced to move at the piston velocity. This causes an important reversed flow velocity near the cylinder wall and gives rise to a boundary layer flow separation from the cylinder wall. Consequently, a secondary negative vortex is

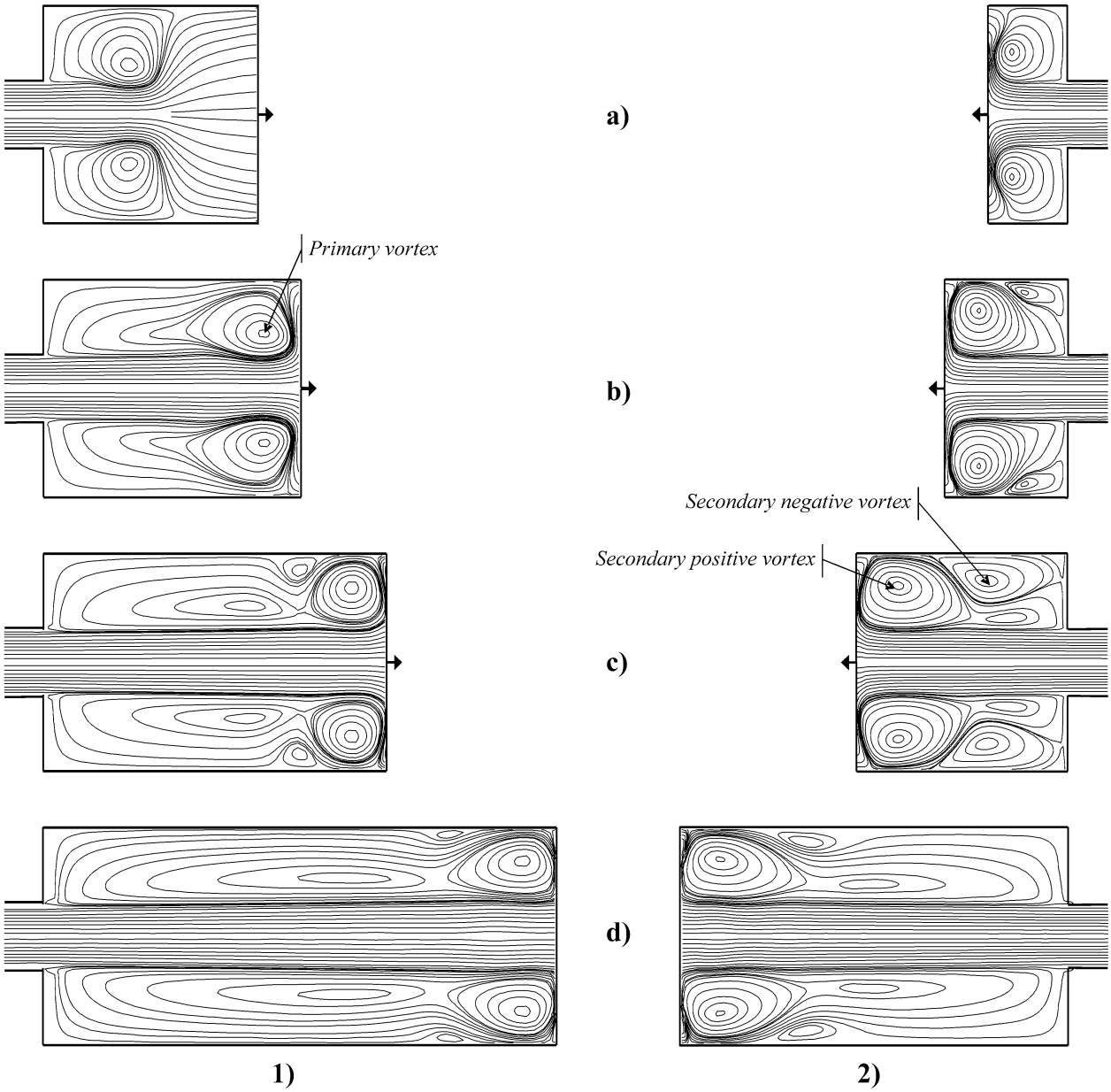

Fig. 6. Streamline patterns for different initial clearances (L_0) during the intake stroke ($Re = 100$, $\alpha = 0.3$): (1) $L_0 = 45$ mm; (2) $L_0 = 9$ mm: (a) 12.5%, (b) 25%, (c) 50%, (d) 100% of the piston stroke (C).

formed close the cylinder wall as sketched in Fig. 5(1(c)). This secondary negative vortex compresses the primary vortex in the r-direction forming a secondary positive vortex inside it. As the expansion ratio α increases the emergence of the secondary negative and positive vortices takes place later and their sizes are smaller.

Fig. 6, presents the streamline patterns for different initial clearances L_0 and for different instants of the intake stroke. For large clearance volume, the primary vortex has a larger distance to travel until it reaches the piston region. Consequently, the reversed flow velocity near the cylinder wall is still small. So only a weak secondary recirculating flow was formed as sketched in Fig. 6(2(a)). On the other hand, when the initial clearance becomes smaller, the primary vortex reaches quickly the piston region. As it reaches the cylinder wall, this vortex is then forced to move at the piston velocity. This causes an important reversed flow velocity near the cylinder wall. This gives rise to a boundary layer flow, which could now strongly separate from the sidewall under the action of the adverse pressure gradient, induced by the main vortex itself. Consequently, viscous and adverse pressure gradient effects become important, so that a secondary vortex is formed close the cylinder wall (Fig. 6(2(c))). This new vortex structure has the opposite sign of the primary vortex. In other words, it represents a negative vorticity region.

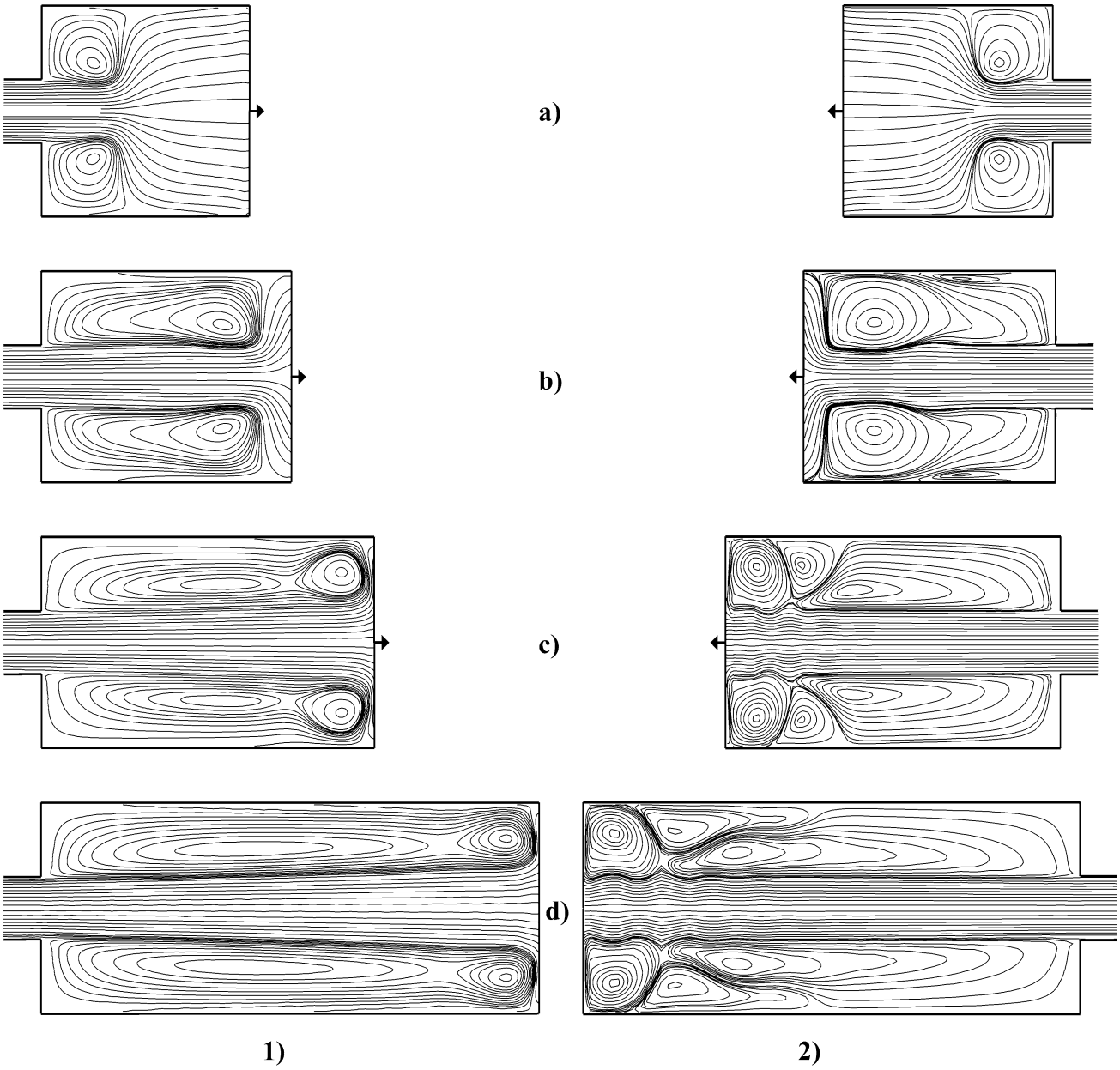

Fig. 7. Streamline patterns for different Reynolds numbers during the intake stroke ($L_0 = 45$ mm, $\alpha = 0.3$): (1) $Re = 50$; (2) $Re = 200$: (a) 12.5%, (b) 25%, (c) 50%, (d) 100% of the piston stroke (C).

We can also note the formation of another secondary vortex near the centreline. This vortex is created by the division of the primary vortex into an additional vortex structure of the same sign (Fig. 6(1(c)) and (1(d))). This positive secondary vortex is formed as a result of the axial elongation of the primary vortex towards the piston region and its compression by the secondary negative vortex in the r-direction. The smaller is the initial clearance the more the vortex stretching is slowed by the rise of the secondary negative vortex.

Fig. 7, presents the streamline patterns for different piston velocity (Reynolds number) and for different instants of the intake stroke. For small Reynolds number, the reversed flow velocity near the cylinder wall is not sufficiently important and only a weak secondary positive vortex is formed near the centreline region (Fig. 7(1)). When Reynolds number becomes important, two secondary vortexes are formed. As depicted in Fig. 7(1(c)) and (2(c)), the size of the first secondary vortex situated near the cylinder wall increase with Reynolds number.

3.2. Thermal field

Figs. 8, 9 and 10 present the thermal fields at different piston locations corresponding to 12.5%, 25%, 50% and

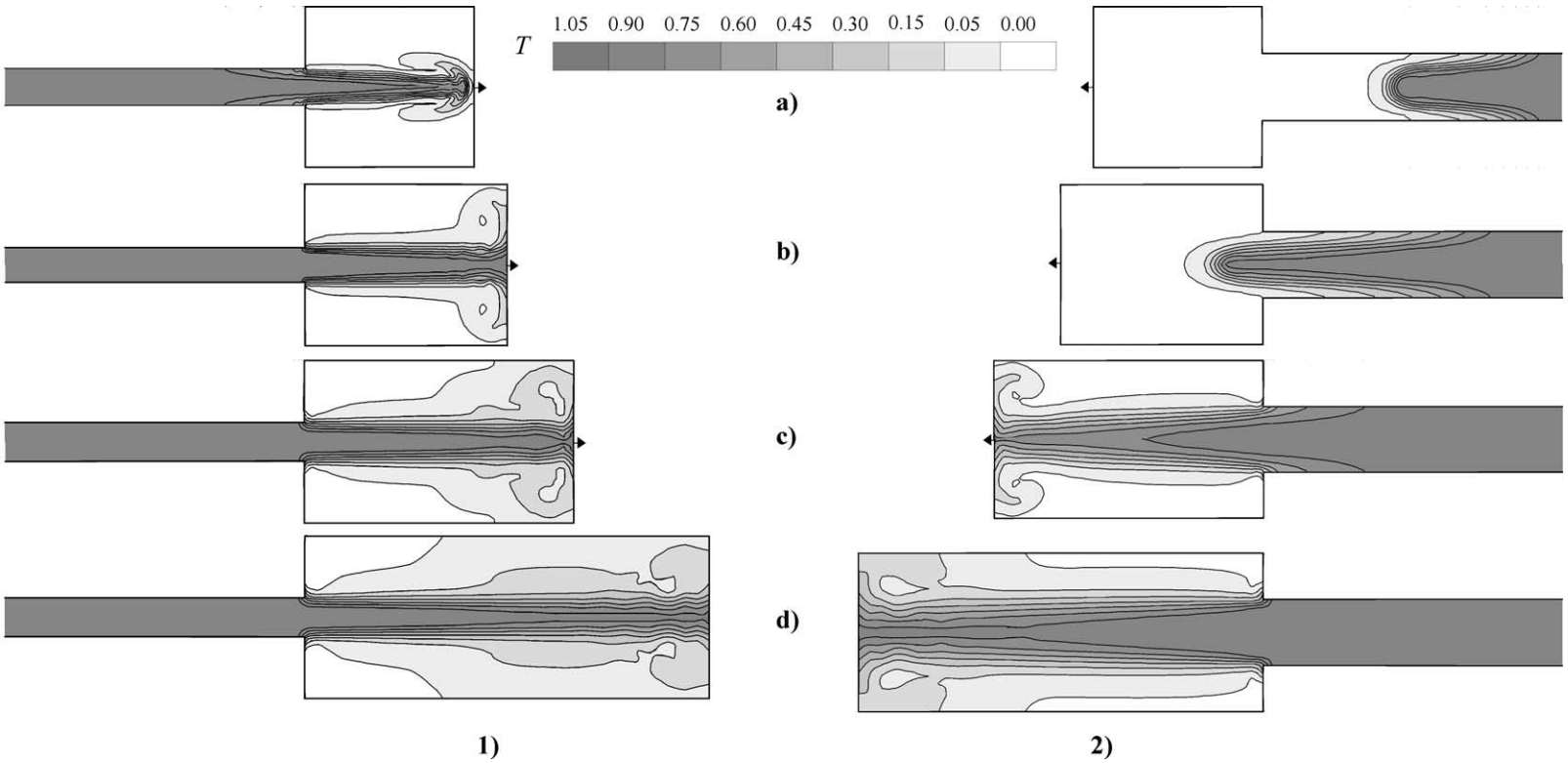

Fig. 8. Temperature fields for different expansion ratios (α) during the intake stroke ($Re = 100$, $L_0 = 45$ mm): (1) $\alpha = 0.2$; (2) $\alpha = 0.4$: (a) 12.5%, (b) 25%, (c) 50%, (d) 100% of the piston stroke (C).

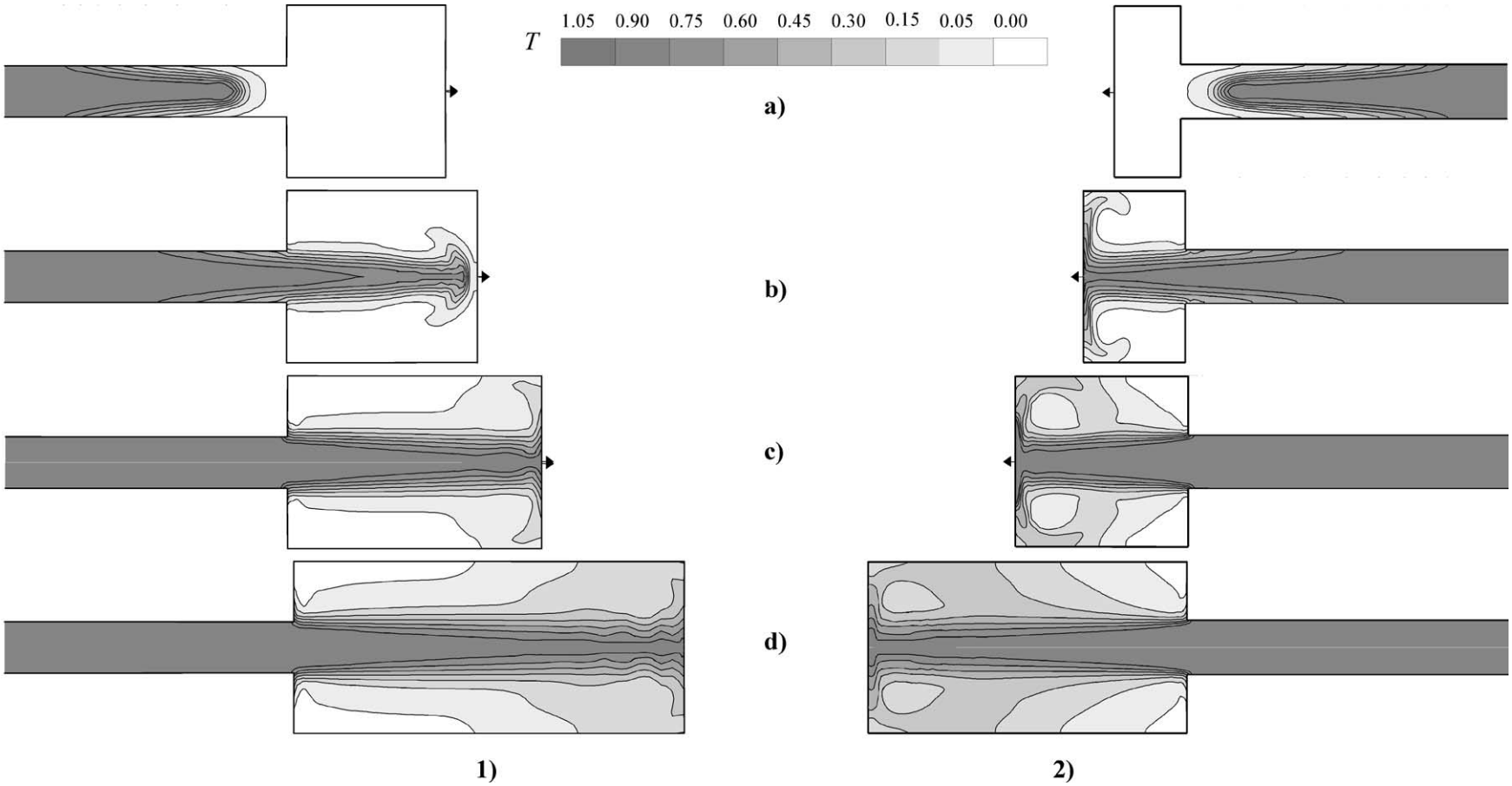

Fig. 9. Temperature fields for different initial clearances (L_0) during the intake stroke ($Re = 100$, $\alpha = 0.3$): (1) $L_0 = 45$ mm; (2) $L_0 = 9$ mm: (a) 12.5%, (b) 25%, (c) 50%, (d) 100% of the piston stroke (C).

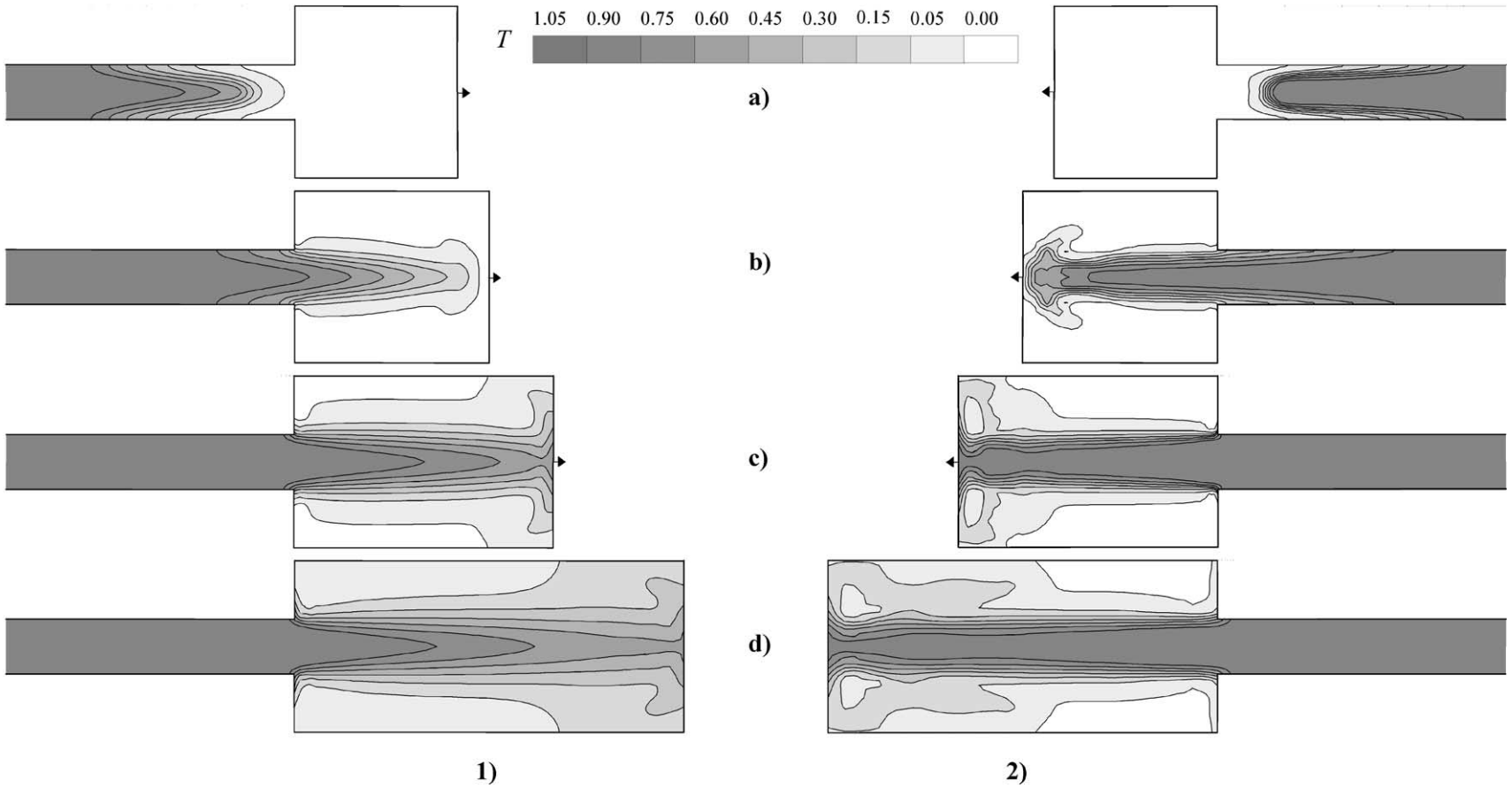

Fig. 10. Temperature fields for different Reynolds numbers during the intake stroke ($L_0 = 45$ mm, $\alpha = 0.3$): (1) $Re = 50$; (2) $Re = 200$: (a) 12.5%, (b) 25%, (c) 50%, (d) 100% of the piston stroke (C).

100% of the total piston stroke, and for different values of expansion ratio α, clearance volume L_0 and Reynolds number, respectively.

Qualitatively the heat transfer during the intake stroke is explained as follows: the fluid sucked through the inlet-pipe is hotter than the fluid initially present in the piston cylinder assembly. As the piston moves, the hot fluid spreads progressively first into the inlet-pipe and then inside the larger pipe. According to the dynamic field the high temperature fluid elements reaches the centreline region more rapidly than the lateral wall region. When the hot fluid elements reaches the piston, they are entailed by the primary vortex towards the cylinder lateral wall. As consequence, the hot fluid elements are forced to move around the vortex, so the core of the recirculating region has a weaker temperature than the region surrounding it.

Fig. 8 presents the predicted thermal fields for different expansion ratios ($\alpha = 0.2$ and $\alpha = 0.4$). The hot fluid progression is more rapid as the axial velocity at the inlet pipe entrance ($z = 0$) increases. Knowing that this velocity is inversely proportional to the square of the inlet pipe radius (Eq. (3)), we can conclude that the progression of the hot fluid is more rapid as the expansion ratio decreases. Thus, the hot fluid elements reach more rapidly the piston region by decreasing the expansion ratio α. Consequently, the heat transfer from the piston head to the lateral wall, by the mean of the primary vortex, occurs more rapidly.

The effect of the initial clearance on the heat transfer in the larger pipe, during the intake stroke, can be seen on Fig. 9. For each case of initial clearance L_0, the piston stroke is the same. Thus, the total hot fluid mass sucked through the intake pipe is also the same. However, for a small initial clearance, the hot fluid elements reach more rapidly the piston region. As a result, the heat convection from the piston head region to the lateral wall region, by the mean of the vortex, takes place more rapidly (Fig. 9(1(d)) and (2(d))). Near the flow impact on the piston, the temperature decreases with the initial clearance volume increase. For high initial clearance, as the negative secondary vortex vanish, the thermal field becomes more homogeneous.

Fig. 10, presents the depicted thermal field for different values of Reynolds numbers. At the beginning of the intake stroke, for a high Reynolds number the axial inlet velocity is greater so that the hot fluid elements reach the piston region more rapidly than for a lower Reynolds number. Consequently, the heat convection from the piston head region to the lateral wall region, by the mean of the primary vortex, takes place more rapidly (Fig. 10(1(b)) and (2(b))).

For a high Reynolds number, the secondary negative vortex emerges nearly before 50% of the total piston stroke near the cylinder wall. This secondary vortex prevents the hot fluid element to come near the lateral wall. Therefore, the wall region closes to this vortex will be still at a weaker temperature than the neighbouring region (Fig. 10(2(c)) and (2(d))). We can conclude that as the Reynolds number increases, the heat convection from the piston head region to the lateral wall region is slowed by the mean of the secondary negative vortex.

As depicted by Fig. 10 and for a high Reynolds number, the core of the primary vortex is still at a weaker temperature. As can be seen, the thermal field is more homogeneous for lower Reynolds number. In fact, in one hand the heat conduction arises for a fixed piston position during a period as longer as the Reynolds number is lower. Therefore, the heat conduction effect becomes important when the Reynolds number decreases and reduces space-variation of temperature near the piston and the lateral wall region. In other hand, when the Reynolds number decreases the secondary negative vortex vanish and the flow becomes more homogeneous.

3.3. Convective heat flux at the entrance of the larger pipe

The order of magnitude of the convective heat flux at the entrance of the larger pipe is far more important than that the diffusive one. So we have presented only the instantaneous convective heat flux *Fc* and the total convected heat *Fct* at the entrance of the larger pipe ($z = L_1$) for different expansion ratios α (Fig. 11), for different Reynolds numbers (Fig. 12) and for different initial clearances L_0 (Fig. 13).

$$Fc = \int_0^{R_1} U(r, L_1)\big[T(r, L_1) - T_0\big]2\pi r \,\mathrm{d}r, \qquad Fct = \int_0^t Fc \,\mathrm{d}t$$

These two quantities are of great interest in some applications where it is necessary to have an idea on the amount of heat that can be sucked during piston stroke.

To better explain the different parameters effects on the instantaneous convective heat flux and the total convected heat, the velocity and the temperature profiles at $z = L_1$ are presented for different piston locations.

As depicted by Figs. 11, 12 and 13 the instantaneous convective heat flux *Fc* and the total convected heat *Fct* are null at the beginning of the intake stroke, before the hot fluid reach the entrance of the larger pipe. When the hot fluid reaches the larger pipe, *Fc* and *Fct* grow as the piston moves. Since a certain piston stroke, the temperature profile at the larger pipe inlet becomes nearly uniform and equal to the inlet temperature. Consequently, the instantaneous convective heat flux *Fc* tends to a constant asymptotic value and the total convected heat *Fct* increases linearly with the piston stroke.

When the expansion ratio decreases (Fig. 11), the hot fluid reaches more rapidly the larger pipe and the temperature, at the larger pipe inlet, approach the inlet one more rapidly. Therefore, the instantaneous convective heat flux *Fc* reaches more rapidly its asymptotic value. At the end of the intake stroke, *Fc* becomes nearly independent of the expansion ratio α. This evolution of the instantaneous convective heat flux explains the decrease of the total convected heat *Fct* with the expansion ratio α.

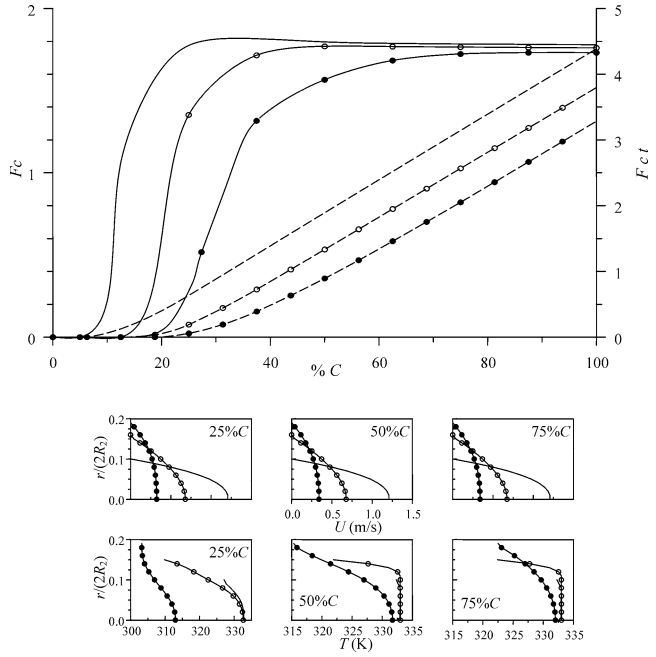

Fig. 11. Instantaneous Convective heat flux *Fc* and total convected heat *Fct* at the entrance of the larger pipe for different expansion ratios $L_0 = 45$ mm, $Re = 100$: *Fc*: —— $\alpha = 0.2$, —○— $\alpha = 0.3$, —●— $\alpha = 0.4$; *Fct*: - - - - - $\alpha = 0.2$, - -○- - $\alpha = 0.3$, - -●- - $\alpha = 0.4$.

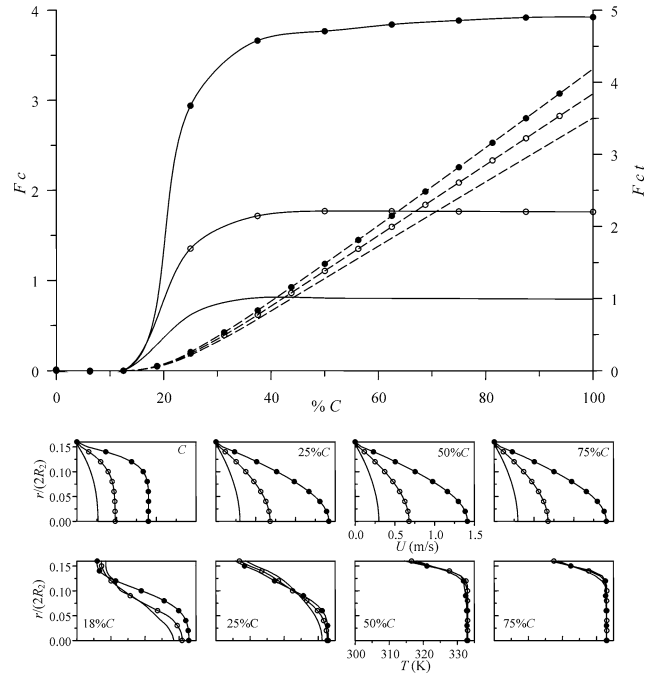

Fig. 12. Instantaneous Convective heat flux *Fc* and total convected heat *Fct* at the entrance of the larger pipe for different Reynolds numbers $L_0 = 45$ mm, $\alpha = 0.3$: *Fc*: —— $Re = 50$, —○— $Re = 100$, —●— $Re = 200$; *Fct*: - -, - - - $Re = 50$, - -○- - $Re = 100$, - -●- - $Re = 200$.

As depicted by Fig. 12, at a fixed piston stroke, *Fc* and *Fct* increase with the Reynolds number. This can be justified by the velocity and the temperature profiles.

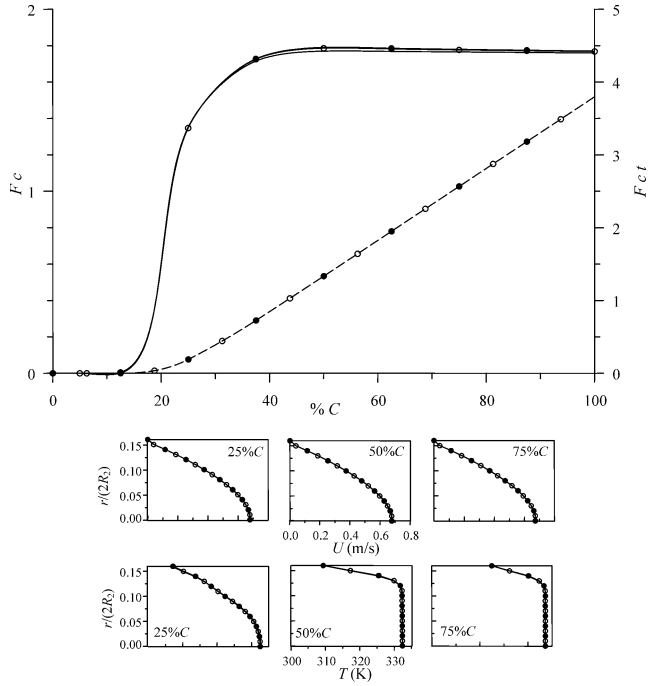

Fig. 13. Instantaneous Convective heat flux *Fc* and total convected heat *Fct* at the entrance of the larger pipe for different initial clearances $Re = 100$, $\alpha = 0.3$: *Fc*: —— $L_0 = 45$ mm, —○— $L_0 = 15$ mm, —●— $L_0 = 9$ mm; *Fct*: - - - - -, $L_0 = 45$ mm, - -○- - $L_0 = 15$ mm, - -●- - $L_0 = 9$ mm.

As shown in Fig. 13, the velocity and the temperature profiles, at the larger pipe inlet, are at each piston stroke nearly independent of the initial clearance L_0. Consequently, at each piston stroke, the instantaneous convective heat flux *Fc* and the total convected heat *Fct* are almost not affected by the initial clearance values.

4. Conclusions

The piston-driving heat transfer and fluid flow in a cylinder containing a sudden expansion was numerically investigated during the intake stroke. The solution method is based on a control-volume-based finite element method using a staggered and moving grid. The streamline patterns and the thermal fields are analysed to evaluate the effect of the expansion ratio, the initial clearance and the piston velocity (Reynolds number) on the heat transfer and the structure of the fluid flow. The effects of these parameters on the instantaneous convective heat flux and on the total convected heat are also evaluated at the sudden expansion section.

The vortexes emergence, stretch, and splitting depend on the expansion ratio, the initial clearance, and the Reynolds number (piston velocity).

As the expansion ratio and the initial clearance decrease or the Reynolds number increase, viscous and adverse pressure gradient effects become important, so that a secondary vortexes are formed close the cylinder wall and inside the primary vortex in the centreline region. The time of the ap-

pearance of these secondary vortices is function of the expansion ratio, the initial clearance volume and the piston velocity or the Reynolds number.

The thermal fields show that the hot fluid progression is more rapid as the expansion ratio decreases. For a small initial clearance the temperature at the flow impact on the piston is higher and the heat convection from the piston head region to the lateral wall region, by the mean of the primary vortex, takes place more rapidly. However, the rising of the secondary negative vortex prevents the hot fluid element to come near the lateral wall so this region is at a weaker temperature than the neighbouring region. The thermal field is more homogeneous for low Reynolds number and high initial clearance volume.

For the same piston stroke, the instantaneous convective heat flux and the total convected heat, at the entrance of the larger pipe, increases with the Reynolds number, decreases with the expansion ratio α and are almost not affected by the initial clearance L_0.

References

[1] J.B. Heywood, Fluid motion within the cylinder of internal combustion engines—The 1986 freeman scholar lecture, ASME J. Fluids Engrg. 109 (1) (1987) 3–35.

[2] B. Ahmadi-Befrui, A.D. Gosman, Assessment of variants of the k–ε turbulence model for engine flow applications, Internat. J. Numer. Methods Fluids 9 (1989) 1073–1086.

[3] B. Farhanieh, L. Davidson, B. Sudén, Employment of second-moment closure for calculation of turbulent reciprocating flows in complex geometries with collocated variable arrangement, Internat. J. Numer. Methods Fluids 16 (1993) 525–544.

[4] Y. Mao, M. Buffat, D. Jeandel, Simulation of the turbulent flow inside the combustion chamber of a reciprocating engine with a finite element method, ASME J. Fluids Engrg. 116 (1994) 363–369.

[5] F. Durst, J.C.F. Pereira, G. Scheuerer, Calculations and experimental investigations of the laminar unsteady flow in a pipe expansion, in: E.H. Hirschel (Ed.), Finite Approximations in Fluid Mechanics, Vieweg, Braunschweig, 1986, pp. 43–55.

[6] H. Ströll, F. Durst, M. Peric, J.C.F. Pereira, G. Scheuerer, Study of laminar, unsteady piston-cylinder flows, ASME J. Fluids Engrg. 115 (1993) 687–693.

[7] H. Ströll, F. Durst, M. Peric, G. Scheuerer, Numerical study of a piston-driven unsteady flow in a pipe with sudden expansion, Internat. J. Numer. Methods Fluids 21 (1995) 237–251.

[8] B.R. Baliga, S.V. Patankar, A new finite-element formulation for convection–diffusion problems, Numer. Heat Transfer 3 (1980) 393–409.

[9] B.R. Baliga, S.V. Patankar, A control-volume finite element method for two-dimensional fluid flow and heat transfer, Numer. Heat Transfer 6 (1983) 245–261.

[10] G.E. Schneider, M.J. Raw, Control-volume finite-element method for heat transfer and fluid flow using collocated variables—1. Computational procedure, Numer. Heat Transfer 11 (1987) 363–390.

[11] C. Masson, H.J. Saabas, B.R. Baliga, Co-located equal-order control-volume finite element method for two-dimensional axisymmetric incompressible fluid flow, Internat. J. Numer. Methods Fluids 18 (1994) 1–26.

[12] A. Omri, S. Ben Nasrallah, Control volume finite element numerical simulation of mixed convection in an air-cooled cavity, Numer. Heat Transfer Part A 36 (6) (1999) 615–638.

[13] M. Peric, R. Kessler, G. Scheuerer, Comparison of finite-volume numerical methods with staggered and colocated grids, Comput. Fluids 16 (1988) 389–403.

[14] S.V. Patankar, D.B. Spalding, A calculation procedure for heat, mass and momentum transfer in three-dimensional parabolic flows, Internat. J. Heat Mass Transfer 15 (1972) 1787–1806.

[15] N. Alleborn, K. Nandakumar, H. Raszillier, F. Durst, Further contributions on the two-dimensional flow in a sudden expansion, J. Fluid Mech. 330 (1997) 169–188.

[16] S. Tavoularis, R.K. Singh, Vortex detachment and reverse flow in pulsatile laminar flow through axisymmetric sudden expansions, J. Fluid Engrg. 121 (1999) 574–579.

[17] K.J. Hammad, M.V. Ötügen, E.B. Arik, A PIV study of the laminar axisymmetric sudden expansion flow, Experiments in Fluids 26 (1999) 266–272.